Tellus (2006), 58B, 418–426
Printed in Singapore. All rights reserved

TELLUS

The effect of sea-ice growth on air–sea CO_2 flux in a tank experiment

By DAIKI NOMURA1*, HISAYUKI YOSHIKAWA-INOUE[1] and TAKENOBU TOYOTA[2],
[1]*Graduate School of Environmental Science and Faculty of Environmental Earth Science, Hokkaido University, Kita-10, Nishi-5, Kita-ku, Sapporo 060-0810, Japan;* [2]*Institute of Low Temperature Science, Hokkaido University, Kita-19, Nishi-8, Kita-ku, Sapporo 060-0819, Japan*

(Manuscript received 14 January 2006; in final form 12 June 2006)

ABSTRACT

In order to clarify the CO_2 exchange between the seawater and the overlying air during the sea-ice formation, we have carried out tank experiments in a low-temperature room. CO_2 concentration above the sea-ice began to increase since the beginning of the sea-ice formation, and increased at larger rates with time and the decrease in air temperature. This increase of CO_2 concentration in air was mainly caused by the increase in dissolved inorganic carbon concentration in the brine of the upper part of sea-ice, changes in CO_2 solubility and dissociation constants of carbonic acid. The CO_2 flux increased logarithmically with time, and reached a level of 2×10^{-4} to 5×10^{-4} g-C m^{-2} hr^{-1} at 50 mm ice thickness. We found that the CO_2 flux was correlated well with the salinity and negatively with the volume of the brine in the upper part of the sea-ice. These suggested the larger role of the difference in partial pressure of CO_2 between brine and air as compared to that of competitive change in the brine volume. Present results suggest the necessity to examine the CO_2 exchange between the seawater and air in seasonal sea-ice areas.

1. Introduction

In high latitudes, oceans are covered with sea-ice whose extent of surface area varies seasonally within a range of 3–6% of the earth's surface (Comiso, 2003), and the impacts of sea-ice cover on the global environment are significant. For example, sea-ice increases albedo, which implies an increase of short-wave solar radiation that has simply been reflected back to space from the surface. Discharge of brine from sea-ice to seawater leads to dense water formation, which plays an important role in determining ocean circulation and transferring carbon from the surface to the abyssal depths of the ocean (Wakatsuchi, 1983; Wakatsuchi and Ono, 1983; Anderson et al., 2004; Hoppema, 2004).

From the viewpoint of geochemical cycles, sea-ice has been considered to impede the gas exchange between the ocean and atmosphere (Tison et al., 2002 and references cited therein). Hence, no carbon cycle models have included CO_2 exchange between the two through sea-ice. However, there have been a few studies that report the possibility of gas exchange through the sea-ice. For example, Gosink et al. (1976) noted that, unlike ice formed from pure or freshwater, sea-ice is a highly permeable medium for gases when the surface temperature is higher than -15°C. They evaluated the rate of penetration for gases (CO_2, sulphur hexafluoride, perfluoromethyl bromide and perfluoroethyl bromide) through the grain boundaries in sea-ice, and briefly discussed the mechanism involved in this process. Tison et al. (2002) indicated the gas composition change in the bubbles of sea-ice during ice formation and melting on the basis of tank experiments, and discussed the mechanism controlling the composition of the bubbles.

Extensive sea-ice provides a unique habitat for polar biological assemblages such as summer algal blooms, which significantly affects the oceanic carbon cycle as well as the polar marine ecology (Arrigo, 2003). In the Arctic Ocean, a drawdown of partial pressure of CO_2 (pCO_2) in surface seawater occurs from winter to spring/summer because of biological activities (Semiletov, 1999; Pipko et al., 2002). Semiletov et al. (2004) show that sea-ice melt ponds and open brine channels act as an important sink for atmospheric CO_2 that must be included in Arctic regional CO_2 budget. In the Southern Ocean, there is a disagreement on estimates of air–sea CO_2 flux. For example, the estimate using a combination of direct and climatologically derived pCO_2 measurements which were mainly on the basis of Austral summer data ranged from 0.5 to 0.7 Gt-C yr^{-1} (Takahashi et al., 2002). On the other hand, the atmospheric

*Corresponding author.
e-mail: daiki@ees.hokudai.ac.jp
DOI: 10.1111/j.1600-0889.2006.00204.x

(Rayner et al., 1999) and oceanic inverse models (Gloor et al., 2003) gave lower atmospheric CO_2 uptakes of about 0.1 Gt-C yr^{-1}. A flux of about 0.1 Gt-C yr^{-1} was determined from the total dissolved inorganic carbon (DIC) and the total alkalinity (TA) in seawater by including winter-time data (McNeil et al., 2005). These studies suggest the necessity of better understanding of the Southern Ocean winter-time CO_2 flux, including the effect of sea-ice existence.

In this paper, in order to clarify the CO_2 exchange mechanism and quantify CO_2 flux during sea-ice formation, we carried out the tank experiments by using natural seawater in a low-temperature room. We present direct evidence for CO_2 release from sea-ice by measuring the CO_2 concentration in the air quasi-continuously, the DIC concentration, and the physical properties of sea-ice. Processes controlling CO_2 flux through the sea-ice are discussed in detail.

2. Experiment

2.1. Apparatus

The CO_2 measuring system consists of a sea-ice formation tank, a non-dispersive infrared gas (NDIR) analyser (LI-6262, LI-COR Inc., Lincoln, USA), a chemical desiccant column [$Mg(ClO_4)_2$, CDC], an electric dehumidifier (ED), solenoid valves (SV), a diaphragm pump, a mass flow controller (MFC), a pressure gauge and a data-acquisition unit connected to a personal computer (PC) (left panel in Fig. 1). The squared sea-ice formation tank (300 × 300 × 650 mm, right panel in Fig. 1) has been installed in the low-temperature room. The tank is made of transparent acrylic boards with 10 mm thickness and surrounded by the insulator with 100 mm thickness to avoid freezing from the side of the tank. We installed a stirrer under the sea-ice formation tank and put a magnetic spinbar at the bottom of the tank to provide homogeneous physical/chemical properties of seawater.

Sample seawater used in this experiment was collected off the eastern coast of Hokkaido, the northern area of Japan and in the sub-Arctic gyre of the western North Pacific. The salinity of coastal water is relatively low (29.89–31.20), and high (33.45) in the western North Pacific. Seawater was injected into the tank up to 550 mm height from the bottom (49.5 L), and the top of the tank was covered with an acrylic board (320 × 320 × 10 mm) attached with Teflon tube connectors that introduce sample air into the NDIR analyser's cell via the 1/4 inch Teflon tube. In order to avoid any effects of pressure change during the sea-ice formation on measurements of air CO_2 concentration in the headspace of the tank, an aluminium bag (2 L, GL Science Inc., Tokyo, Japan.) has been used as a pressure regulator, and installed at the outlet of the NDIR analyser.

In a closed circuit shown by the solid thick line (left panel in Fig. 1), air was circulated at a flow rate of 125 ml min^{-1}. In order to determine the CO_2 concentration precisely, it is necessary to measure the sample air at the same condition as that of standards. Prior to A/D integration of output voltage, we stopped the airflow for 25 s to establish temperature equilibrium in the NDIR analyser's cell. The small effect of pressure on measurements of CO_2 concentration was corrected by the relationship between output voltage of the NDIR analyser and pressure in the sample cell of the analyser. Four standards (typically 324, 341, 363 and 406 ppm CO_2 in natural air) traceable to the WMO mole fraction scale (Inoue and Ishii, 2005) were used to calibrate the CO_2 measuring system prior to the sea-ice formation experiment.

2.2. Methods of experiment

Before sea-ice formation, air temperature in the low-temperature room was kept constant at −1.3 °C (or +1.0 °C), and CO_2 concentration in dry air equilibrated with seawater was adjusted to be in the range from 216 to 292 ppm by adding small amounts of H_3PO_4 or NaOH solution. Then we preserved the seawater for 2 d, which was enough to establish equilibrium between the seawater and overlying air. After the confirmation of constant CO_2 concentration in the air of the headspace (±2.5 ppm), the experiment was initiated (elapsed time = 0 hr) by decreasing

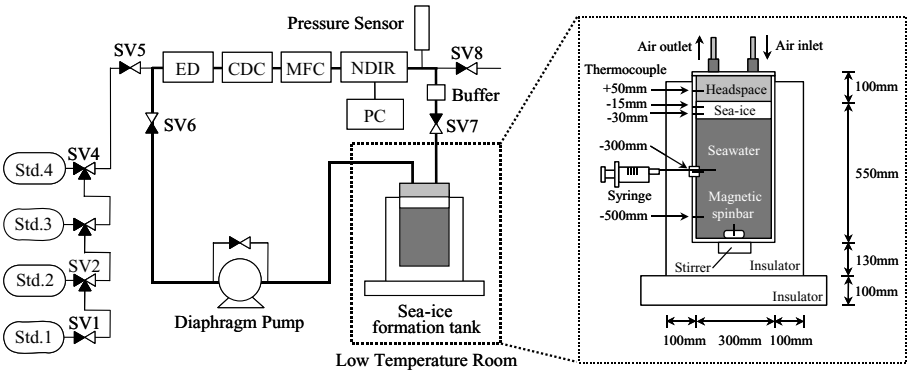

Fig. 1. Schematic diagrams of the CO_2 measuring system (left panel) and sea-ice formation tank (right panel). In the left panel, solid thick lines indicate the closed circuit that flows air to measure the CO_2 concentration in the headspace of the tank.

room temperatures from −1.3 °C (+1.0 °C) to those ranging from −15 °C to −30 °C. For each experiment, the sea-ice thickness grew up to about 50 mm to evoke natural sea-ice/seawater conditions (Toyota, 1998). CO_2 concentration in the air has been measured at 10 min intervals.

To examine the effect of salinity on the CO_2 release from sea-ice, we conducted an experiment by using fresh water. Prior to ice formation from fresh water, CO_2 equilibrium between the water and overlying air was established, and room temperature decreased from +1.0 °C to −25 °C. To avoid the destruction of the sea-ice formation tank as a result of high pressures of the ice from fresh water, we stopped the ice formation when its thickness became about 30 mm.

The temperatures at 300 mm above the tank, at 50 mm above the seawater surface (in the headspace of the tank), and at water depths of 15, 30, 300 and 500 mm were measured by copper-constantan thermocouples every 10 min. Sea-ice thickness was measured visually every 3 hr.

The seawater samples for measurements of salinity (10 ml) were taken carefully through a rubber cap placed 300 mm below the seawater surface by using a plastic syringe every 6 hr. This was stored in a room at ordinary temperature for a few days, and salinity was measured with a TOA SALT ANALYZER SAT-210 (TOA Electronics Ltd., Tokyo, Japan). Standard deviation for measurements of salinity was estimated to be 0.03 ($n = 15$).

The seawater samples for measurements of DIC (120 ml) were sampled after the establishment of chemical equilibrium. DIC concentration was determined by the coulometry technique (Johnson et al., 1985). Working seawater standards traceable to the Certified Reference Material distributed by Prof A. G. Dickson (Scripps Institution of Oceanography, USA) were used to calibrate the DIC measuring system (Wakita et al., 2003). Analytical precision (1σ) was estimated to be 1.5 μmol kg^{-1} based on duplicate seawater samples ($n = 8$).

At the end of the experiment, a piece of sea-ice (150 mm × 150 mm × about 50 mm) was removed, and kept in another low-temperature room of −15 °C for a few days until it was ready for analysis (Toyota, 1998). Two pieces of the sea-ice sample with 50 × 50 mm were then made by using an electric band saw, and each piece was divided into three layers: the upper layer with 15 mm thickness (layer 1), middle layer with 20 mm thickness (layer 2) and bottom layer with 15 mm thickness (layer 3). We measured the sea-ice bulk volume, weight and salinity after melting to calculate the average brine volume fraction (F_b) in sea-ice for the two pieces by equations following Cox and Weeks (1983) and Eicken (2003).

The brine volume fraction can be derived as:

$$F_b \equiv \frac{V_b}{V} = \frac{\rho S_i}{\rho_b S_b}, \tag{1}$$

where V_b is the brine volume, V is the sea-ice bulk volume, ρ is the sea-ice bulk density and S_i is the salinity after melting. In a temperature range higher than −23 °C, brine salinity (S_b) and density (ρ_b) in g cm^{-3} as a function of sea-ice temperature and salinity can be approximated by the following:

$$\rho_b = 1 + 8 \times 10^{-4} S_b, \tag{2}$$

$$S_b = \left(1 - \frac{54.11}{T}\right)^{-1} \times 1000, \tag{3}$$

where T is the temperature in °C.

3. Results & discussion

3.1. Experimental conditions

Table 1 summarizes the experimental conditions used for respective experimental runs. In this work, we conducted experiments at four different room temperatures. After decreasing room temperature from −1.3 °C to −15 °C for Exp. 1, −20 °C for Exp. 2-A and 2-B, −25 °C for Exp. 3-A, 3-B and 3-C, and −30 °C for Exp. 4, the room temperature was kept constant during the experiment. The room temperature decreased from +1.0 °C to −25 °C for Exp. 3-D and 3-E. Air temperature in the headspace of the tank was higher than that in the low-temperature room. This is caused by the heat transfer from seawater to air.

After decreasing the room temperature (elapsed time = 0 hr), it took 3.3–7.8 hr for the sea-ice formation tank to form sea-ice at the seawater surface, except in Exp. 3-D, where it took 11.8 h as a result of high seawater temperature (+1.0 °C) when room temperature was decreased. The ice thickness increased almost rectilinearly because ice thickness was very thin in our experiment (Wakatsuchi, 1983). The growth rate of sea-ice was calculated to be within the range from 0.9 to 1.8 mm hr^{-1} (Table 1) depending on the air temperature in the headspace, and these values were approximately the same as those in the Okhotsk Sea (Toyota et al., 2004).

Changes in the seawater salinity during the experiment (ΔS) increased as a result of drainage of the high saline water (brine) expelled via the brine channel. ΔS values showed large variability for each experiment, and there were no correlations with the ice growth rate (Table 1). Unfortunately, during the experiments, there occurred a small amount of sea-ice formation (about 5 mm thickness) on the side and bottom of the sea-ice formation tank, caused by heat transfer from seawater to room air via the insulator. Hence, salt balance calculated from seawater and surface sea-ice volume, salinities and densities were not established.

3.2. Air CO_2 concentration

Increases in CO_2 concentration in the air before and after the sea-ice formation (ΔCO_2) were plotted against time in Fig. 2. The time when ΔCO_2 began to increase agreed well with the beginning of sea-ice formation. CO_2 concentration increased at a larger growth rate with the growth of sea-ice, increasing by

Table 1. Experimental conditions for each experiment

	Temperature, °C				Sea-ice growth rate ± *SE*, mm hr^{-1} [c] (r^2)	Sea-ice thickness, mm	ΔS
	Room	Headspace	[a]Seawater	[b]Sea-ice			
Exp. 1	−15.3	−7.0	−2.0 to −2.4	−2.7 to −2.5	0.9 ± 0.05 (0.96)	45	2.66
Exp. 2-A	−20.2	−8.7	−1.7 to −2.2	−3.1 to −2.9	1.4 ± 0.04 (0.99)	50	3.23
Exp. 2-B	−21.8	−7.8	−1.9 to −2.2	−3.3 to −2.6	1.5 ± 0.18 (0.96)	55	3.23
Exp. 3-A	−25.9	−9.9	−1.8 to −2.4	−3.8 to −2.8	1.6 ± 0.09 (0.98)	53	3.61
Exp. 3-B	−25.6	−10.0	−1.6 to −2.3	−3.9 to −3.1	1.6 ± 0.10 (0.96)	55	2.27
Exp. 3-C	−25.8	−10.4	−1.5 to −2.4	−3.8 to −3.1	1.8 ± 0.12 (0.95)	53	3.04
Exp. 3-D	−26.6	−10.0	−2.1 to −2.5	−3.8 to −3.4	1.3 ± 0.15 (0.96)	53	3.19
Exp. 3-E	−24.4	−9.0	−0.2 to −0.3	–	–	30	0
Exp. 4	−30.7	−10.7	−1.8 to −2.5	−4.1 to −3.3	1.7 ± 0.13 (0.96)	50	3.09

[a]Seawater temperatures at the beginning of sea-ice formation ranged from −0.2 °C to −2.1 °C, which was caused by the rapid cooling near the surface, and super-cooling of seawater (Wakatsuchi, 1974). At the end of the experiment, the seawater temperature was about −2.4 °C, except for Exp. 3-E, due to super-cooling of seawater (Toyota, 1998).
[b]Temperatures at 15 and 30 mm below the sea-ice surface at the end of experiment.
[c]r^2 indicates the squared correlation coefficients of the linear fitting for estimations of sea-ice growth rate.

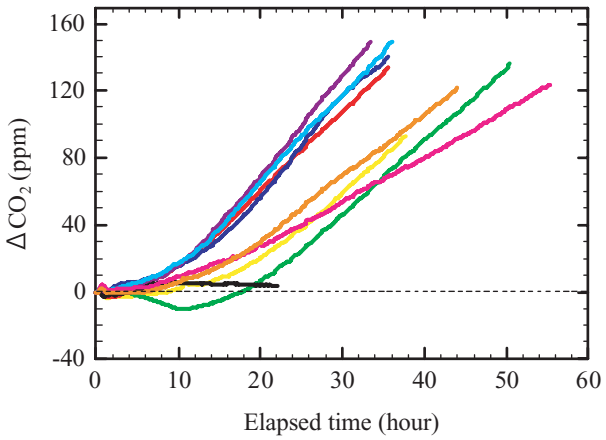

Fig. 2. Time-series of the CO_2 concentration in the air above the sea-ice for Exp. 1 (—pink), Exp. 2-A (—orange), Exp. 2-B (—yellow), Exp. 3-A (—light blue), Exp. 3-B (—red), Exp. 3-C (—blue), Exp. 3-D (—yellow green), Exp. 3-E (—black), and Exp. 4 (—purple). ΔCO_2 indicates the increase in CO_2 concentration since the beginning of decreasing room temperature to form the sea-ice. The horizontal dashed line indicates the $\Delta CO_2 = 0$ ppm.

Table 2. CO_2 concentration in the air before and after ice formation, and DIC concentration and salinity in seawater prior to sea-ice formation

Experiment	[a]CO_2, ppm	Δ CO_2, ppm	Elapsed time, hour	DIC, μmol kg^{-1}	Salinity
Exp 1	235.1	123.8	55.3	2181.8	30.96
Exp 2-A	257.1	121.1	44.0	2112.6	30.60
Exp 2-B	291.4	92.5	37.7	2159.3	33.45
Exp 3-A	226.0	149.3	36.0	2379.1	31.20
Exp 3-B	287.5	133.7	35.7	-	30.02
Exp 3-C	215.9	139.6	35.7	-	29.89
Exp 3-D	269.7	136.1	50.5	2196.6	33.45
Exp 3-E	261.0	[b]3.5	22.2	55.3	0
Exp 4	236.6	149.3	33.5	2117.5	31.08

[a]CO_2 concentration in dry air equilibrated with seawater at −1.3 °C or +1.0 °C (Exp. 3-D and Exp. 3-E)*.
[b]CO_2 concentration increased by 5.5 ppm at the beginning of ice formation (see text).
*pCO_2 can be calculated by multiplying a factor of about 0.994.

90–150 ppm at the end of the experiment (Table 2) except for Exp. 3-E. For Exp. 3-E, at the beginning of ice formation, ΔCO_2 increased slightly (5.5 ppm). During ice formation, ΔCO_2 was constant within the range of 1.3 ppm. The slight increase in ΔCO_2 at the beginning of ice formation might be caused by the same process that occurred during sea-ice formation. Before cooling the room temperature (elapsed time < 0), the CO_2 concentration in the air equilibrated with the seawater was constant for all experiments. After cooling, ΔCO_2 decreased slightly due to the temperature effect on pCO_2 in seawater (4.23% °C^{-1}; Takahashi et al., 2002).

If no outgas occurred from the brine, the relative increase in DIC concentration will be equal to that of salinity, which would lead to a significantly high pCO_2 value. By measuring two variables describing the carbonate system in seawater, we could calculate the pCO_2 in the brine/seawater during the sea-ice formation. The CO_2 solubility was given as a function of temperature ranging from −1°C to 40°C and salinity from 0 to 40 (Weiss, 1974). Equilibrium constants of carbonic acids were also given as a function of temperature from 0°C to 45°C and salinity from 5 to 45 (see e.g. DOE, 1994; Millero, 1995). For all experiments, brine salinity was higher than 42

Table 3. The brine salinity and brine volume fraction for each experiment

	Brine salinity: S_b			Brine volume fraction : F_b, %		
Experiment	Layer 1	Layer 2	Layer 3	Layer 1	Layer 2	Layer 3
Exp. 1	48.1	45.7	43.2	15.5	16.4	19.2
Exp. 2-A	56.7	51.7	46.6	13.8	16.0	22.3
Exp. 2-B	59.9	51.0	41.9	–	–	–
Exp. 3-A	68.5	56.6	44.4	12.4	12.6	23.5
Exp. 3-B	73.6	58.6	43.0	13.8	12.9	20.4
Exp. 3-C	69.8	58.6	47.0	13.3	14.0	22.4
Exp. 3-D	68.0	61.6	55.1	–	–	–
Exp. 4	75.2	62.4	49.3	9.7	13.5	22.3

(Table 3) and sea-ice (brine) temperature was lower than −2°C (Table 1). The equilibrium constants reported earlier as functions of temperature and salinity may have lead to the results that deviated fairly largely at conditions during sea-ice formation, but would help us to discuss changes in pCO_2 at least quasi-quantitatively. As examples, we have calculated the pCO_2 in the brine existing in layer 1 of Exp. 1 and that of Exp. 4. Due to the condensation effect of DIC and changes in solubility and dissociation constants, the pCO_2 increased by 203 μatm from 234 μatm for layer 1 of Exp. 1 and by 667 μatm from 235 μatm for that of Exp. 4. During the sea-ice formation, salinity of seawater below sea-ice increased by 2.7 to 3.6 (Table 1). The pCO_2 in seawater increased by 28 μatm for Exp. 1 and 32 μatm for Exp. 4, which are smaller than the increase of air CO_2 concentration observed for each experiment. These results show a predominant role of the brine in sea-ice by adding CO_2 to the air in the headspace.

Previous work for sea-ice formation experiments in the laboratory reported an abiotic drop in pH in the brine with ionic strength, and a smaller increase in DIC concentration in the brine as compared with salinity (Papadimitriou et al., 2003). The sea-ice formed in this work is expected to be permeable for gases since surface temperature was higher than −15°C (Gosink et al., 1976).

In addition to the changes in DIC concentration, equilibrium constants and CO_2 solubility, $CaCO_3$ precipitation can result in enrichment of CO_2 (Anderson and Jones, 1985; Killawee et al., 1998; Marion, 2001; Papadimitriou et al., 2003):

$$Ca^{2+} + 2HCO_3^- \rightarrow C_aCO_3 + H_2O + CO_2. \quad (4)$$

In our experiment, the temperature in sea-ice was within the range of which the precipitation of $CaCO_3$ could occur. But, the concentration of phosphate, which interferes the precipitation of $CaCO_3$ (Killawee et al., 1998) was also high because we used the coastal seawater, sub-Arctic surface water in the western North Pacific, and H_3PO_4 solution to adjust pCO_2 in seawater. At the moment, we have no data that allow us to discuss the precipitation of $CaCO_3$. If the precipitation of $CaCO_3$ took place in the brine, the pCO_2 was higher than that calculated from solubility and dissociation constants. A good reproducibility conducted at different concentrations of DIC and pCO_2 in seawater suggests the relatively minor role of $CaCO_3$ precipitation in determining the CO_2 flux through the sea-ice.

The present results show that pCO_2 in the brine is extremely high when compared with that of seawater bulk. Therefore, gas bubbles trapped in sea-ice can be expected to contain a high concentration of CO_2 (Miyake and Matsuo, 1963; Tison et al., 2002).

3.3. *CO_2 flux from sea-ice to overlying air*

We calculated the CO_2 flux from sea-ice to the headspace of the tank by using changes in the CO_2 concentration measured every 10 min. The time series of CO_2 flux for each experiment during sea-ice formation were plotted in Fig. 3. The CO_2 flux increased at a larger rate initially, and tended to increase gradually during the rest of the experiment. The CO_2 flux occurred largely with decreases in air temperature. We fitted the CO_2 flux data to the logarithmic function to evaluate the magnitude of CO_2 flux at the same thickness of sea-ice formed at different temperature (Table 4).

Here, we examined the relationships between the CO_2 flux at 50 mm thickness and brine salinity and brine volume fraction for each layer. The CO_2 flux at 50 mm thickness versus brine salinity at layer 1 is shown in Fig. 4a. CO_2 fluxes at 50 mm were correlated well with brine salinity of layers 1 and 2, but not for layer 3 ($r^2 = 0.79$ for layer 1, $r^2 = 0.66$ for layer 2 and $r^2 = 0.07$ for layer 3; data not shown for layers 2 and 3). Next, the flux versus brine volume fraction at layer 1 is also shown in

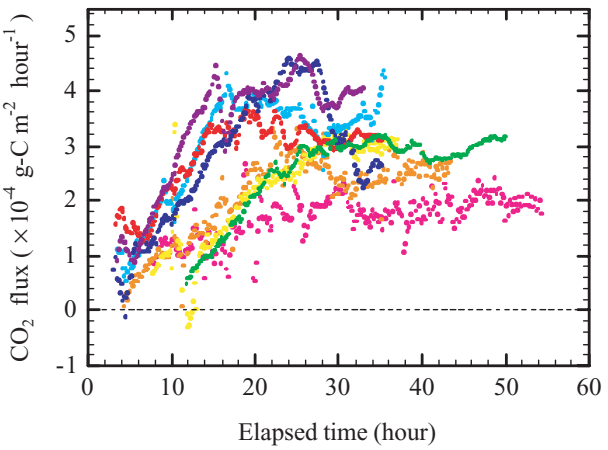

Fig. 3. Time-series of the CO_2 flux for Exp. 1 (—; pink), Exp. 2-A (—; orange), Exp. 2-B (—; yellow), Exp. 3-A (—; light blue), Exp. 3-B (—; red), Exp. 3-C (—; blue), Exp. 3-D (—; yellow green), Exp. 4 (—; purple). The horizontal dashed line indicates the CO_2 flux = 0 g-C m^{-2} hr^{-1}.

Table 4. The CO_2 flux expressed as logarithmic functions of time and CO_2 flux at a thickness of 50 mm

Experiment	[a]Equation	[b]r^2	[c]CO_2 flux $\pm$ *SE*, g-C m^{-2} hr^{-1}
Exp. 1	0.5 ln (t) +3.6 $\times$ 10^{-3}	0.49	(2.1 $\pm$ 0.03) $\times$ 10^{-4}
Exp. 2-A	1.1 ln (t) −1.3	0.76	(2.8 $\pm$ 0.04) $\times$ 10^{-4}
Exp. 2-B	2.0 ln (t) −3.9	0.71	(3.5 $\pm$ 0.10) $\times$ 10^{-4}
Exp. 3-A	1.4 ln (t) −1.0	0.74	(4.0 $\pm$ 0.06) $\times$ 10^{-4}
Exp. 3-B	0.9 ln (t) +0.2	0.71	(3.5 $\pm$ 0.04) $\times$ 10^{-4}
Exp. 3-C	1.6 ln (t) −1.6	0.65	(3.9 $\pm$ 0.08) $\times$ 10^{-4}
Exp. 3-D	1.6 ln (t) −2.8	0.77	(3.4 $\pm$ 0.06) $\times$ 10^{-4}
Exp. 4	1.7 ln (t) −1.3	0.83	(4.6 $\pm$ 0.06) $\times$ 10^{-4}

[a]Equation was expressed as logarithmic function with time (t), since the beginning of sea-ice formation.
[b]The value r^2 indicates the squared correlation coefficient(s) for the least-squares fitting of the logarithmic function.
[c]CO_2 flux at 50 mm ice thickness.

Fig. 4b. The two were negatively correlated well at layers 1 and 2, and not for layer 3 ($r^2 = 0.81$ for layer 1, $r^2 = 0.69$ for layer 2 and $r^2 = 0.48$ for layer 3).

Without sea-ice, the CO_2 flux between the seawater and overlying air (J) can be estimated by the product of the gas transfer velocity (k), solubility of CO_2 (α, Weiss, 1974), and difference in pCO_2 between the seawater and air:

$$J = k\alpha \left(\mathrm{pCO_2^{sw}} - \mathrm{pCO_2^{a}}\right), \tag{5}$$

where superscript 'sw' means the seawater and 'a' the air. Equation 5 is based on the fact that CO_2 transfer between seawater and air is controlled by processes in the near-surface water (Liss, 1973). If the processes determining the CO_2 flux from the sea-ice occur near the surface of brine existing in the upper part of sea-ice (Fig. 4), we could use the follow equation to express the CO_2 flux,

$$J = r_\mathrm{b} k\alpha \left(\mathrm{pCO_2^{b}} - \mathrm{pCO_2^{a}}\right), \tag{6}$$

where r_b is the ratio of surface of the brine channel to sea-ice surface, which is probably proportional to the volume fraction, F_b, and $pCO_2{}^\mathrm{b} - pCO_2{}^\mathrm{a}$ is the difference in pCO_2 between the brine and air. The CO_2 flux increased along with the increase of the difference in pCO_2 between the brine and the air (Fig. 5) although r_b of layer 1 was expected to decrease. This indicates a larger contribution of the difference in pCO_2 between the two phases to the CO_2 flux. If we assume that the value of r_b is equal to that of F_b, we can determine the gas transfer velocity. In the film model of gas transfer developed by Whitman (1923), the gas transfer velocity can be related to the thickness of the film (z) by $k = D/z$, where D is the molecular diffusion coefficient of CO_2 in water (Broecker and Peng, 1982). While the experimental results of air–water gas transfer do not support the film model to express the processes between the water and the air (Holmen and Liss, 1984; Wanninkhof, 1992), the film thickness gives us a clue concerning the rate-determining step of CO_2 transfer from the sea-ice. The thickness of the film was calculated to be less than a few hundred micrometres (Broecker and Peng, 1982), which rationalizes the use of Eq. (6).

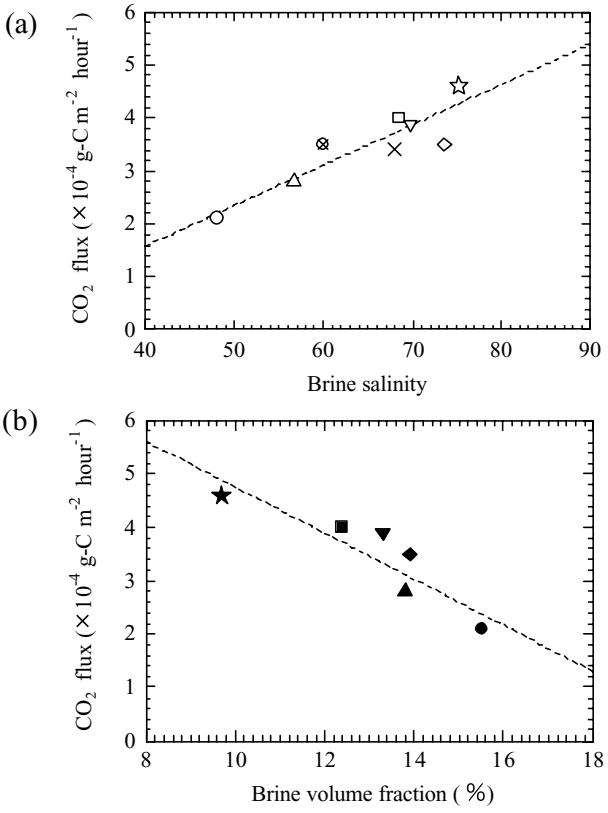

Fig. 4. (a) CO_2 flux at 50 mm thickness versus brine salinity at layer 1 for Exp. 1 (open circle), Exp. 2-A (open triangle), Exp. 2-B (open cross circle), Exp. 3-A (open square), Exp. 3-B (open diamond), Exp. 3-C (open reverse triangle), Exp. 3-D (cross), and Exp. 4 (open star). Dashed line indicates the linear fitting line for each experiment ($r^2 = 0.79$). (b) CO_2 flux at 50 mm thickness versus brine volume fraction at layer 1 for Exp. 1 (solid circle), Exp. 2-A (solid triangle), Exp. 3-A (solid square), Exp. 3-B (solid diamond), Exp. 3-C (solid reverse triangle), and Exp. 4 (solid star). Dashed line indicates the linear fitting line for each experiment ($r^2 = 0.81$).

By using a buffer factor β and the relationship between DIC and salinity discussed above, Eq. (6) can be expressed as

$$J = r_\mathrm{b} k\alpha \left\{\mathrm{pCO_2^0}\beta \left(S_\mathrm{b} - S^0/S^0\right) - \left(\mathrm{pCO_2^a} - \mathrm{pCO_2^0}\right)\right\}. \tag{7}$$

In Eq. (7), superscript 0 means $t = 0$, the time when chemical equilibrium between the seawater and the air was established. Equation 7 indicates that the CO_2 flux is proportional to the relative increase in salinity. The present experiment shows a good relationship between CO_2 flux at the same sea-ice thickness and brine salinity in the upper layer (Fig. 4a), which is partly due to the relatively large contribution of the first term of the

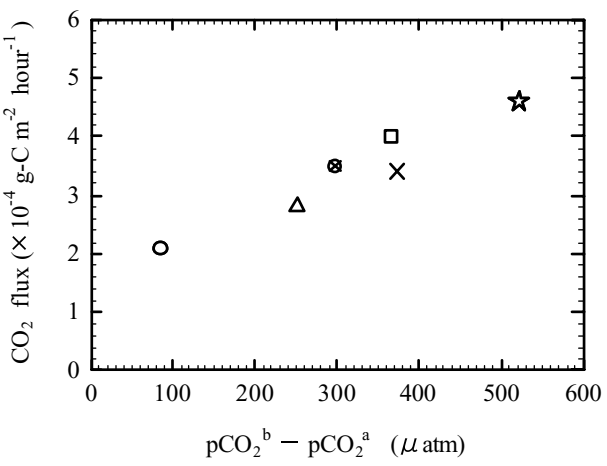

Fig. 5. CO_2 flux at 50 mm thickness versus the difference in pCO_2 between brine and overlying air ($pCO_2{}^b - pCO_2{}^a$) at the end of the experiment for Exp. 1 (open circle), Exp. 2-A (open triangle), Exp. 2-B (open cross circle), Exp. 3-A (open square), Exp. 3-D (cross), and Exp. 4 (open star). $r_b k$ calculated from the difference in pCO_2 between brine and overlying air at the end of the experiment, seawater solubility and CO_2 flux was 0.32 cm hr^{-1} for Exp. 1, 0.14 cm hr^{-1} for Exp. 2-A, 0.15 cm hr^{-1} for Exp. 2-B, 0.14 cm hr^{-1} for Exp. 3-A, 0.12 cm hr^{-1} for Exp. 3-D, 0.12 cm hr^{-1} for Exp. 4. $pCO_2{}^a$ was calculated by assuming barometric pressure of 1 atm and saturated water vapor of brine in layer 1 (Weiss and Price, 1980).

right-hand side of Eq. (7) and the fairly same value of $pCO_2{}^0/S^0$ for each experiment. In order to discuss the CO_2 flux during sea-ice formation more quantitatively, data about variations in r_b and $pCO_2{}^b$ are needed.

We estimate the amount of CO_2 transferred from the sea-ice to the air during the sea-ice formation at an air temperature of -10°C (Table 1), and compared it with the total amount of DIC in seawater and brine. At the end of the experiment, about 0.06% of carbon in seawater (49.5 L) was released to the air. Assuming conservative properties of DIC, we evaluated its amount in seawater that became sea-ice by using eqs. (1)–(3), and volumes and densities of sea-ice/seawater. The amount of CO_2 transferred to the air corresponded to 0.8% of the total amount of DIC in seawater that became sea-ice. About one third (32.3%) remained in the sea-ice, and two-thirds (66.9%) were injected into the seawater below the sea-ice due to drainage of the brine.

Present results suggest CO_2 release from the sea-ice to the air during the sea-ice formation period in high latitudes; however, there are only few data that allow us to evaluate variations in CO_2 flux from the sea-ice. If we use the average CO_2 flux at an air temperature of -10°C (3.7×10^{-4} g-C m^{-2} hr^{-1}) listed in Table 4, the surface area and duration of sea-ice growth period (Comiso, 2003), we could calculate the CO_2 flux from the sea-ice in both hemispheres. The amount of CO_2 released from sea-ice was calculated to be 13 Mt-C yr^{-1} in the Northern Hemisphere (10×10^{10} m^2, 150 d) and 31 Mt-C yr^{-1} in the Southern Hemisphere (16.5×10^{10} m^2, 210 d). This is an example when we use the experimental CO_2 flux of 3.7×10^{-4} g-C m^{-2} hr^{-1} to calculate the amount of CO_2 release from sea-ice in high latitudes. However, the calculated CO_2 flux in both hemispheres shed light on the importance of CO_2 budget during the sea-ice formation process. It is necessary to measure CO_2 exchange between the seawater and the overlying air in sea-ice formation/melting area to understand the carbon budget in high latitudes in both hemispheres.

4. Summary

In order to clarify the CO_2 exchange between the seawater and overlying air during sea-ice formation and the factors controlling it, we have carried out tank experiments in a low-temperature room, installing an ice formation tank made of acryl (300 × 300 × 650 mm). The top of the acrylic tank was covered with an acrylic board to measure the CO_2 concentration in the air above the sea-ice. During the formation of sea-ice frozen from natural seawater (49.5 L), we measured the CO_2 concentration in the air (10 L) by using a NDIR analyser installed outside of the low-temperature room.

To evoke natural sea-ice/seawater conditions, we made sea-ice at a growth rate ranging from 0.9 to 1.8 mm hr^{-1} until its thickness became 50 mm. The growth rate of sea-ice was controlled by changing the air temperature in the low-temperature room from -15°C to -30°C. At these conditions, the air temperature above the sea-ice became -7.0°C to -10.7°C.

The CO_2 concentration above the sea-ice began to increase since the beginning of sea-ice formation, and increased largely against unit increases in time, and the decrease in air temperature above the sea-ice. At a sea-ice thickness of 50 mm, CO_2 concentration increased by 90 to 150 ppm. During the sea-ice formation, the salinity of seawater increased by 2.7 to 3.6, which led to the increase of CO_2 concentration by 28 to 32 ppm (DOE, 1994; Millero, 1995). This CO_2 was considered to be released from the brine through the brine channel. The larger increase of CO_2 concentration during sea-ice formation occurred due to the increase in DIC concentration in the brine of the upper part of sea-ice, changes in CO_2 solubility and dissociation constants of carbonic acid, and possibly by the precipitation of $CaCO_3$.

The CO_2 flux from the sea-ice to the air increased logarithmically with time, and reached to the level of 2×10^{-4} to 5×10^{-4} g-C m^{-2} hr^{-1} at 50 mm sea-ice thickness. The present results show that the CO_2 flux increased along with the difference in pCO_2 between brine and air in spite of decreases in the brine volume. During the sea-ice formation, less than 1% of the total amount of DIC in seawater that became sea-ice was transferred to the air. The present results suggest that sea-ice growth acts as a CO_2 source for the atmosphere and is not a simple insulator for CO_2 exchange between the sea and overlying air. At the moment, however, we do not know the CO_2 flux from the seasonal

sea-ice in high latitudes; therefore, it is necessary to examine the CO_2 exchange between the seawater and the air in the seasonal sea-ice formation area.

5. Acknowledgements

The authors would like to express heartfelt thanks to Drs T. Kawamura, S. Noriki, Y. W. Watanabe, K. Suzuki, K. Shirasawa, N. Tanaka, S. Tsunogai and Y. Nakano for their useful comments and providing the measurement device of sea-ice. This work is partly supported by the Japan Society for the Promotion of Science (#17654089 and #16310001).

References

Anderson, L. G., Falck, E., Jones, E. P., Jutterström, S. and Swift, J. H. 2004. Enhanced uptake of atmospheric CO_2 during freezing of seawater: a field study in Storfjorden, Svalbard. *J. Geophys. Res.* **109**, doi:10.1029/2003JC002120.

Anderson, L. G. and Jones, E. P. 1985. Measurement of total alkalinity, calcium, and sulfate in natural sea ice. *J. Geophys. Res.* **90**, 9194–9198.

Arrigo, K. R. 2003. Primary production in sea ice. In: *Sea Ice—An Introduction to Its Physics, Chemistry, Biology and Geology* (eds.D. N. Thomas and G. S. Dieckmann). Blackwell Science, Oxford, pp. 143–183.

Broecker, W. S. and Peng, T.-H. 1982. The atmospheric imprint. The cycles of gases within the sea. In: *Tracers in the Sea*. LDGO Press, New York, pp. 110–161.

Comiso, J. C. 2003. Large-scale characteristics and variability of the global sea ice cover. In: *Sea Ice—An Introduction to Its Physics, Chemistry, Biology and Geology* (eds.D. N. Thomas and G. S. Dieckmann). Blackwell Science, Oxford, pp. 112–142.

Cox, G. F. N. and Weeks, W. F. 1983. Equation for determining the gas and brine volumes in sea-ice samples. *J. Glaciol.* **29**, 306–316.

DOE 1994. In: *Handbook of Methods for the Analysis of the Various Parameters of the Carbon Dioxide System in Sea Water; Version 2* (eds.A. G. Dickson and C. Goyet) ORNL/CDIAC-74. Oak Ridge National Laboratory, Oak Ridge, Tennessee.

Eicken, H. 2003. From the microscopic, to the Microscopic, to the regional scale: growth, microstructure and properties of sea ice. In: *Sea Ice—An Introduction to Its Physics, Chemistry, Biology and Geology* (eds.D. N. Thomas and G. S. Dieckmann). Blackwell Science, Oxford, pp. 22–81.

Gloor, M., Gruber, N., Sarmiento, J., Sabine, C. L., Feely, R. A. and co-authors. 2003. A first estimate of present and preindustrial air-sea CO_2 flux patterns based on ocean interior carbon measurement and models. *Geophys. Res. Lett.* **30**, 1, doi:10.1029/2002GL015594.

Gosink, T. A., Pearson, J. G. and Kelly, J. J. 1976. Gas movement thorough sea-ice. *Nature* **263**, 41–42.

Holmen, K. and Liss, P. 1984. Models for air-water gas transfer: an experimental investigation. *Tellus* **36B**, 92–100.

Hoppema, M. 2004. Weddell Sea is a globally significant contributor to deep-sea sequestration of natural carbon dioxide. *Deep-Sea Res. I* **51**, 1169–1177.

Inoue, H. Y. and Ishii, M. 2005. Variations and trends of CO_2 in the surface seawater in the Southern Ocean south of Australia between 1969 and 2002. *Tellus* **57B**, 58–69.

Johnson, K. M., King, A. E. and Sieburth, J. M. 1985. Coulometric TCO_2 analysis for marine studies: an introduction. *Mar. Chem.* **16**, 61–82.

Killawee, J. A., Fairchild, I. J., Tison, J. L., Janssens, L. and Lorrain, R. 1998. Segregation of solutes and gases in experimental freezing of dilute solution: implications for natural glacial systems. *Geochim. Cosmochim. Acta* **62**, 3637–3655.

Liss, P. S. 1973. Processes of gas exchange across an air-water interface. *Deep-Sea Res.* **20**, 221–238.

Marion, G. M. 2001. Carbonate mineral solubility at low temperatures in the Na-K-Mg-Ca-H-Cl-SO_4-OH-HCO_3-CO_3-CO_2-H_2O system. *Geochim. Cosmochim. Acta* **65**, 1883–1896.

McNeil, B. I., Metzl, N., Key, R. M., and Matear, R. J. 2005. An empirical estimate of the Southern ocean air-sea CO_2 flux. Proceeding of the 7th International Carbon Dioxide Conference, Boulder, Colorado.

Millero, F. J. 1995. Thermodynamic of the carbon dioxide system in the oceans. *Geochim. Cosmochim. Acta* **59**, 661–677.

Miyake, Y. and Matsuo, S. 1963. A role of sea ice and sea water in the Antarctic on the carbon dioxide cycle in the atmosphere. *Pap. Meteorol. Geophys.* **14**, 120–125.

Papadimitriou, S., Kennedy, H., Kattner, G., Dieckmann, G. S. and Thomas, D. N. 2003. Experimental evidence for carbonate precipitation and CO_2 degassing during sea ice formation. *Geochim. Cosmochim. Acta,* **68**, 1749–1761.

Pipko, I. I., Semiletov, I. P., Tishchenko, P. Y., Pugach, S. P. and Christensen, J. P. 2002. Carbonate chemistry dynamics in Bering Strait and the Chukchi Sea. *Progr. Oceanogr.* **55**, 77–94.

Rayner, P. J., Enting, I. G., Francey, R. J. and Langenfelds, R. 1999. Reconstructing the recent carbon cycle from atmospheric CO_2, $\delta^{13}C$ and O_2/N_2 observations. *Tellus* **51B**, 213–232.

Semiletov, I. P., Makshtas, A. and Akasofu, S. 2004. Atmospheric CO_2 balance: the role of Arctic sea ice. *Geophys. Res. Lett.* **31**, doi:10.1029/2003GL017996.

Semiletov, I. P. 1999. Aquatic sources and sinks of CO_2 and CH_4 in the polar regions. *J. Atmos Sci.* **56**, 286–306.

Takahashi, T., Sutherland, S. C., Sweeney, C., Poisson, A., Metzl, N. and co-authors. 2002. Global sea-air CO_2 flux based on climatological surface ocean pCO_2, and seasonal biological and temperature effects. *Deep-Sea Res. II* **49**, 1601–1622.

Tison, J. L., Hass, C., Gowing, M. M., Sleewaegen, S. and Bernard, A. 2002. Tank study of physico-chemical controls on gas content and composition during growth of young sea ice. *J. Glaciol.* **48**, 161, 177–191.

Toyota, T. 1998. A study on growth processes of sea ice in the southern region of the Okhotsk Sea, evaluated from heat budget and sea ice sample analysis. Ph. D. dissertation, Institute of Low Temperature Science, Hokkaido University, Sapporo, Japan, p. 143.

Toyota, T., Kawamura, T. and Ohshima, K. I. 2004. Thickness distribution, texture and stratigraphy, and a simple probabilistic model for dynamical thickening of sea ice in the southern Sea of Okhotsk. *J. Geophys. Res.* **109**, doi:10.1029/2003JC002090.

Wakatsuchi, M. 1974. Experiments on the growth of sea ice and the rejection of brine. *Low Temp. Sci.* **A32**, 195–205.

Wakatsuchi, M. 1983. Brine exclusion process from growing sea ice. Ph. D. dissertation, Institute of Low Temperature Science, Hokkaido University, Sapporo, Japan, p. 65.

Wakatsuchi, M. and Ono, N. 1983. Measurements of salinity and volume of brine excluded from growing sea ice. *J. Geophys. Res.* **88**(C5), 2943–2951.

Wakita, M., Watanebe, W. Y., Watanebe, S. and Noriki, S. 2003. Oceanic uptake rate of anthropogenic CO_2 in a subpolar marginal sea: the Sea of Okhotsk. *Geophys. Res. Lett.* **30**, 24, doi:10.1029/2003GL018057.

Wanninkhof, R. 1992. Relationship between wind speed and gas exchange over the ocean. *J. Geophys. Res.* **97**, 7373–7382.

Weiss, R. F. 1974. Carbon dioxide in water and seawater: the solubility of a non-ideal gas. *Mar. Chem.* **2**, 203–215.

Weiss, R. F. and Price, B. A. 1980. Nitrous oxide solubility in water and seawater. *Mar. Chem.* **8**, 347–359.

Whitman, W. G. 1923. The two-film theory of gas absorption. *Chem. Met. Eng.* **29**, 146–148.